Journal of Applied Polymer Science

In situ preparation of polyaniline within neutral, anionic, and cationic superporous cryogel networks as conductive, semi-interpenetrating polymer network cryogel composite systems

Nurettin Sahiner,[1,2] Sahin Demirci[1,2]

[1]Department of Chemistry, Faculty of Science and Arts, Canakkale Onsekiz Mart University, Terzioglu Campus, 17100, Canakkale, Turkey

[2]Nanoscience and Technology Research and Application Center, Canakkale Onsekiz Mart University, Terzioglu Campus, 17100, Canakkale, Turkey

Correspondence to: N. Sahiner (E-mail: sahiner71@gmail.com)

ABSTRACT: Polyaniline [p(An)], one of the most known conducting polymers, was prepared within superporus nonionic polyacrylamide [p(AAm)], anionic poly(2-acrylamido-2-methyl-1-propane sulfonic acid sodium salt) [p(AMPS)], and cationic poly(3-acrylamidopropyltrimethyl ammonium chloride) [p(APTMACl)] cryogels. After they were synthesized, washed, and dried, the neutral p(AAm), anionic p(AMPS), and cationic p(APTMACl) cryogels were soaked in an ammonium persulfate/aniline solution (1:1.25 ratio) in 1 *M* hydrochloric acid for the *in situ* oxidative polymerization of p(An) with the cryogel matrices as templates or reactors. The prepared p(AAm)/p(An), p(AMPS)/p(An), and p(APTMACl)/p(An) semi-interpenetrating polymer network (semi-IPN) conductive cryogel composites were characterized with scanning electron microscopy (SEM), Fourier transform infrared spectroscopy, and conductivity analysis. The SEM images revealed that the superporus cryogel networks were almost completely filled with p(An) conductive polymers (CPs). Among the cryogel–CP semi-IPNs, we found that p(AAm)/p(An) semi-IPN conductive cryogel composites provided the highest conductivity values of $1.4 \times 10^{-2} \pm 4 \times 10^{-4}$ S/cm; this was a 6.4×10^{6} fold increase in the conductivity from the values of $2.2 \times 10^{-9} \pm 1 \times 10^{-10}$ for p(AAm) cryogels. © 2016 Wiley Periodicals, Inc. J. Appl. Polym. Sci. **2016**, *133*, 44137.

KEYWORDS: composites; conducting polymers; porous materials; supramolecular structures; surfaces and interfaces

Received 4 April 2016; accepted 1 July 2016

DOI: 10.1002/app.44137

INTRODUCTION

Conductive polymers (CPs) as organic materials were synthesized for first time in the middle of the 1970s. Apart from metals and inorganic semiconductors, CPs are conjugated polymers with spatially extended π bonding, which confers unique electrical, electrochemical and optical properties.[1–4] CPs have been investigated extensively for biomedical applications, biosensors, neural prostheses electrode applications,[5–9] controlled drug-delivery systems,[10,11] and also applications for the microelectronic industry, such as in photovoltaic devices, electrochromic displays, light-emitting diodes, and even battery technology.[12–14] The most commonly known CPs are polyaniline [p(An)], polypyrrole, polythiophene, poly(*p*-phenylene vinylene), and poly(ethylene dioxythiophene), and among them, p(An) is one of the most used CPs because it is considered the most convenient conducting polymer on account of its basic properties, such as its simple synthesis, enhanced electrochemical behavior, and thermal and relative environmental stability. Because of the relatively good electrical conductivity and high chemical and thermal stability, p(An)-based conducting polymers could be used in electronic devices, actuators, and sensors. P(An) can undergo reversible acid–base doping–dedoping behavior because of its readily controllable properties, including its free volume, solubility, optical activity, and electrical conductivity.[5,15–17] Interestingly, polyelectrolyte hydrogels, such as poly(2-acrylamido-2-methyl-1-propane sulfonic acid sodium salt) [p(AMPS)], poly(3-acrylamidopropyltrimethyl ammonium chloride) [p(APTMACl)], and poly(acrylic acid) [p(AAc)], also provide ionic conductivity because of their ionic-group-developing functional groups.[18–20] In past decades, the hydrogel–CP composites, known as *semi-interpenetrating polymer networks (semi-IPNs)*, have attracted great attention from researchers in different fileds.[21–23] However, novel types of hydrogels, known as *cryogels*, offer very intriguing properties compared to common hydrogels; these properties include a high flexibility, elasticity, superporosity, and fast response to stimuli, and cryogels have been a favorite for the

design of advanced-stimuli responsive systems.[24,25] Recently, cryogels have been used to carry out common hydrogel tasks in many applications, such as templates for *in situ* metal nanoparticle preparation,[26] adsorbents for environmental applications,[27] cell scaffolds or tissues engineering,[28] column filler materials,[29] bioseparation,[30] and the design of biosensing devices.[31]

In this study, we report the synthesis of various types of cryogels, including nonionic polyacrylamide [p(AAm)], anionic p(AMPS), and cationic p(APTMACl) cryogels, as templates for the synthesis of a conducting polymer, p(An). The superporous matrices of these cryogels were used for the *in situ* oxidative polymerization of electroconductive p(An), and the prepared semi-IPN composites were named p(AAm)–p(An), p(AMPS)–p(An), and p(APTMACl)–p(An), respectively. The prepared p(AAm)–p(An), p(AMPS)–p(An), and p(APTMACl)–p(An) semi-IPN conductive cryogels were characterized via scanning electron microscopy (SEM), Fourier transform infrared (FTIR) spectroscopy, and conductivity analysis, and their conductivities were compared. This is the first report in the literature about the use of neutral, anionic, and cationic cryogel networks as templates in the preparation of a conducting polymer to obtain cryogel semi-IPN conductive composites. Cryogels are preferred over conventional hydrogels because of their apparent superior capabilities, such as their mechanical strength; fast response time to external stimuli, such as pH, solute molecules, temperature, and electric field; and inherently superconnected and interconnected pore structures, which offer great advantages for many applications, including absorption, separation, catalysis, and many more in biomedical fields (tissue engineering, hormone–DNA, and drug isolation, removal, and enrichment) over conventional hydrogels.[32–34]

EXPERIMENTAL

Materials

Acrylamide (AAm; 98%, Acros), 2-acrylamido-2-methyl-1-propane sulfonic acid sodium salt (AMPS; 50%, Sigma-Aldrich), and 3-acrylamidopropyltrimethyl ammonium chloride (APTMACl; 75%, Sigma-Aldrich) were used as monomers; *N,N′*-methylene bisacrylamide (MBA; 98%, Sigma-Aldrich) was used as a crosslinker; *N,N,N,N*-tetramethyethylenediamine (TEMED; 98%, Merck) was used as an accelerator; and potassium persulfate (KPS; 98%, Sigma-Aldrich) was used as an initiator in the synthesis of superporous cryogels. Aniline (An; 98%, Sigma-Aldrich) was used as the monomer for the *in situ* synthesis of CP within cryogels, and ammonium persulfate (APS; 98%, Sigma-Aldrich) was used as an oxidation agent in hydrochloric acid (HCl; 36–38%; Sigma-Aldrich) for the oxidative polymerization of An. Acetone and ethanol (technical grade) and distilled (DI) water were used for the washings of the cryogels.

Synthesis of the Superporous Cryogels

Synthesis of the Nonionic p(AAm) Cryogels. The synthesis of the p(AAm) cryogels were done according to the literature with some modifications.[25] In short, 0.5 g of AAm monomer and 6.4% w/v MBA was dissolved in 6.5 mL of DI water in a vial; then, 50 μL of TEMED was added to this mixture and vortexed. The APS initiator solution was prepared in another vial with APS (1 mol % AAm) by the dissolution of a certain amount in 1 mL of DI water. These two vials were placed into a freezer for 3 min; then, the initiator solution was added to the monomer, and the crosslinker and accelerator solutions were mixed and vortexed rapidly. Then, this mixture was placed quickly into plastic straws (∼8 mm in diameter), and the straws were placed in a freezer at −18 °C for 24 h to complete cryopolymerization. After then, the obtained p(AAm) cryogels were cut into identical cylindrical shapes, washed with 500 mL of DI water three times for 1 h each, dried in a freeze dryer, and stored in sealed bags for further use.

Synthesis of the Anionic p(AMPS) Cryogels. The preparation of the p(AMPS) cryogel was also performed according to the literature with some modifications.[26] Briefly, 0.78 mL of an aqueous AMPS solution (50 wt %) and 8.8% w/v MBA was dissolved in 5.22 mL of DI water, and 50 μL of TEMED was added to this monomer solution and mixed with a vortex mixer. Separately, 0.0054 g of KPS (1 mol % of monomer) was dissolved in 1 mL of DI water and cooled in a deep freeze for 3 min. Finally, this initiator solution and the cooled monomer mixture were mixed, and then, this mixture was placed in plastic straws (∼8 mm in diameter). Then, the straws were placed in a deep freezer at −18 °C for 24 h of cryopolymerization. Finally, the obtained anionic cryogels were cut into similar dimensions (∼1 cm). Then, these acquired cryogels were cleaned by washing with 100 mL of DI three times each, dried in a freeze dryer, and stored in sealed bags for further use.

Synthesis of the Cationic p(APTMACl) Cryogels. Again, the APTMACl cryogels were synthesized according to the literature with slight modifications.[27] The cationic monomer of APTMACl weighing 0.832 g, and 16.5% w/v MBA were dissolved in 5.5 mL of DI water. To this solution, 50 μL of TEMED was added and vortexed. In a separate vial, 0.0083 g of KPS initiator solution (1 mol % APTMACl) dissolved in 1 mL of DI water was added, and both vials were placed into a deep freezer for 3 min. Then, these solutions, the initiator solution, and the monomer solution were mixed and quickly placed in plastic straws (∼8 mm in diameter). The straws were placed in a freezer at −18 °C for 24 h to complete the cryopolymerization. Thereafter, the prepared cationic cryogels were cut into identical cylindrical shapes, washed with DI as mentioned previously for the other cryogels, freeze-dried, and stored for further use in a sealed bag.

Synthesis of the p(An) CPs within the Cryogels

The synthesized and dried p(AAm), p(APTMACl), and p(AMPS) cryogels were used as templates for the synthesis of electroconductive p(An) within them. For this purpose, the dried p(AAm), p(AMPS), and p(APTMACl) cryogels were weighed and placed into 10 mL of An for 30 min to load the corresponding network with An. Then, the An-absorbed cryogels were weighed again to determine the amounts of absorbed An. After this, these An-absorbed cryogels were transferred into 50 mL of an 1 *M* HCl solution that contained a 1:1.25 molar ratio of APS to An for the oxidative polymerization of An, and the reaction was carried out by stirring at 250 rpm for 5 h. Then, the obtained p(AAm)–p(An), p(AMPS)–p(An), and p(APTMACl)–p(An) semi-IPN conductive cryogels were washed

with acetone, ethanol, and DI water at least twice each to remove the impurities and free p(An) from the surface of the cryogels. Then, the synthesized p(AAm)–p(An), p(AMPS)–p(An), and p(APTMACl)–p(An) semi-IPN conductive cryogel composites were dried in oven at 50 °C for the characterization studies.

Characterization

SEM images of the bare p(AAm), p(AMPS), and p(APTMACl) cryogels and the p(AAm)–p(An), p(AMPS)–p(An), and p(APTMACl)–p(An) semi-IPN conductive cryogel composites were obtained with SEM (JEOL JSM-5600). Very thin pieces of synthesized and freeze-dried bare p(AAm), p(AMPS), and p(APTMACl) cryogels and p(AAm)–p(An), p(AMPS)–p(An), and p(APTMACl)–p(An) semi-IPN conductive cryogel composites were placed onto carbon-tape-attached aluminum SEM stubs and coated with gold to a few nanometers of thickness *in vacuo* before imaging.

The FTIR spectra of the bare p(AAm), p(AMPS), and p(APTMACl) cryogels and p(AAm)–p(An), p(AMPS)–p(An), and p(APTMACl)–p(An) semi-IPN conductive cryogel systems were recorded between wave numbers 650 and 4000 cm^{-1} with attenuated total reflectance attached FTIR spectrometer (Thermo, Nicolet-iS10).

Conductivity Measurements

The conductivities of the p(AAm), p(AMPS), and p(APTMACl) and their corresponding p(An) containing semi-IPN cryogel systems were calculated from current–voltage measurements via a computer-controlled electrometer (Keithley 2400) at room temperature. Conductive carbon tape was attached at the top and the bottom of the p(AAm), p(AMPS), and p(APTMACl) cryogels and their corresponding p(An)-containing semi-IPN cryogel composites. The effect of template on the conductivities of the synthesized p(AAm)–p(An), p(AMPS)–p(An), and p(APTMACl)–p(An) semi-IPN conducting cryogel composites were investigated.

RESULTS AND DISCUSSION

Synthesis and Characterization of the Conductive p(AAm)–p(An), p(AMPS)–p(An), and p(APTMACl)–p(An) Semi-IPN Conductive Cryogels

Cryogels with innate properties are considered as special types of hydrogels because of their superporous interconnected pore sizes up to a few hundreds of micrometers.[24] Porosity, especially interconnected superporosity in polymeric hydrogels, offers many advantages, such as high elasticity, high mechanical strength, and fast response to exterior stimuli, such as solvent, pH, temperature, or solute molecules, and can provide fast actuation in comparison to common hydrogels.[24] Cryogels of different formulations (e.g., nonionic)[25] and with charge-developing features (e.g., anionic[26] and cationic[27] have been prepared and reported in the literature for different purposes. AAm and its derivatives are among the commonly prepared hydrogels and cryogels.[24–27] The schematic presentation of the synthesis of cryogels of nonionic p(AAm), anionic p(AMPS), and cationic p(APTMACl) cryogels are given in Figure 1(a). Basically, the polymerization and crosslinking of the corresponding monomers were carried out under cryogenic conditions (below the melting point temperature of the solvent, water), so the formed ice crystals during network formation led to superporous and interconnected pores with tunable pore sizes that could be up to a few hundred when the ice crystals were thawed. The SEM images of the synthesized p(AAm), p(AMPS), and p(APTMACl) cryogels are given in Figure 1(b–d), respectively. As shown, the SEM images of the p(AAm), p(AMPS), and p(APTMACl) cryogels revealed that all of the cryogels possessed superporous structures with a 10–100-μm pore size range. Therefore, the use of these superporous structures of the nonionic p(AAm) and anionic p(AMPS), and cationic p(APTMACl) cryogels matrix as templates or constructs for the *in situ* preparation of electroconductive p(An) was reasonable. For this purpose, certain amounts of cleaned and dried p(AAm), p(AMPS), and p(APTMACl) cryogels (0.5 g of each) were placed in 10 mL of An for 30 min to load An into the cryogel networks. The absorbed amount of An for each cryogel was calculated from the weight increase of the cryogels due to An absorption. Then, we placed these An-absorbed p(AAm), p(AMPS), and p(APTMACl) cryogels in 50 mL of a 1 *M* HCl solution that contained a 1:1.25 molar ratio of An to APS according to the An-absorbing capacities of the cryogels under a 250-rpm mixing rate for 3 h for the An polymerization within the p(AAm) and p(AMPS) cryogel networks and for 30 min for the p(APTMACl) cryogel network. The polymerization times of An were found to be much lower for the cationic p(APTMACl) cryogels than for the p(AAm) and p(AMPS) cryogels, as the p(APTMACl) cryogels showed high swellability during the absorption of An into the p(APTMACl) cryogels; this allowed ready diffusion of initiator for fast oxidative polymerization. The digital camera images of bare, An-absorbed, and *in situ* p(An) synthesized p(AAm), p(APTMACl), and p(AMPS) cryogels semi-IPN composites are given in Figure 2(a), (b) and (c) respectively. In Figure 2(a), white-colored bare p(AAm) cryogels turned black for p(AAm)–p(An) semi-IPN conductive cryogels upon *in situ* synthesis of p(An) as an indication of conductive p(An) formation within the network of the cryogels. The white-colored p(AMPS) cryogel was turned black by the synthesis of p(An) within the pores of the p(AMPS) cryogel, as shown in Figure 2(b). Similar observations were also observed, as shown in Figure 2(c), with a change of the brown-colored p(APTMACl) cryogels to black after the *in situ* polymerization of p(An) within the cationic network of the cryogel.

For the characterization of the *in situ* synthesis of the electroconductive p(An) in p(AAm), p(AMPS), and p(APTMACl) cryogels, SEM images of the p(AAm)–p(An), p(AMPS)–p(An), and p(APTMACl)–p(An) semi-IPN conductive composite cryogels were taken and are given in Figure 3. As shown in Figure 3(a), in comparison with Figure 1(b), the porous p(AAm) cryogels were filled with electroconductive p(An), and the pore sizes were assumed to decrease to approximately 5–25 μm from 10–100 μm upon the formation of the p(AAm)–p(An) semi-IPN conductive cryogel composites. The pores of the p(AMPS) cryogels were also almost fully filled with p(An), and the corresponding SEM images are given in Figure 3(b) in comparison to the bare p(AMPS) cryogels, as illustrated in Figure 1(c).

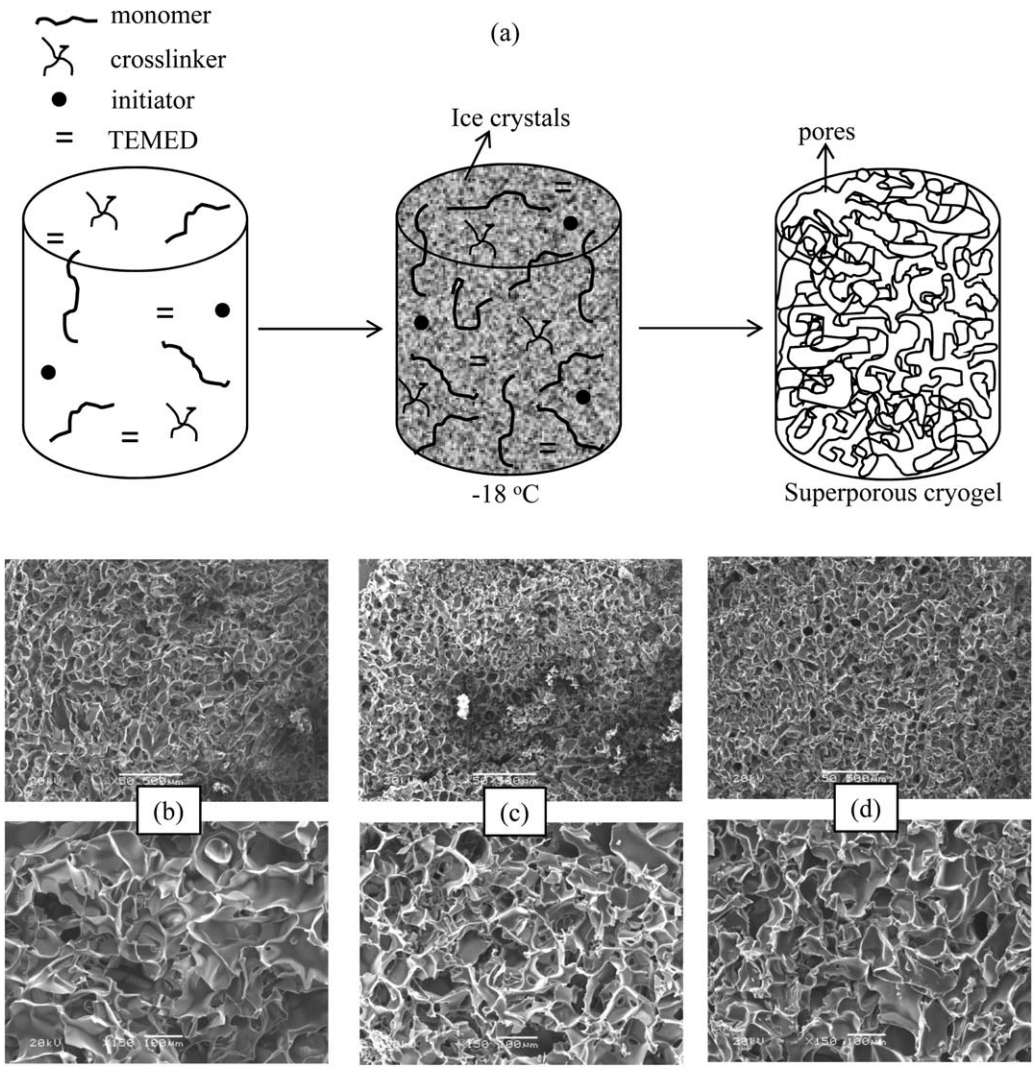

Figure 1. (a) Schematic presentation of the synthesis of cryogels and (b–d) SEM images of p(AAm), p(AMPS), and p(APTMACl) cryogels, respectively, at different magnifications.

Similarly, as demonstrated in Figure 3(c) in comparison to Figure 1(d), the SEM images of the p(APTMACl)–p(An) semi-IPN conductive cryogels showed that pores of the p(APTMACl) cryogels also contained conductive p(An) and the pore sizes decreased from 10–100 μm to a few micrometers.

To further confirm the *in situ* synthesis of p(An) within the pores of p(AAm), p(AMPS), and p(APTMACl) cryogels and the synthesized semi-IPN conductive cryogels, the FTIR spectra of the bare samples and corresponding semi-IPN conductive cryogel composites were taken and compared with each other, as demonstrated in Figure 4(a–c), respectively. In the FTIR spectra of the bare p(AAm) and p(AAm)–p(An) semi-IPN conductive cryogels are presented in Figure 4(a); the characteristic peaks of the p(AAm) cryogel (e.g., the NH_2 stretching peaks for primary amide at 3311 and 3292 cm^{-1}, the aliphatic C—H stretching vibrations at 2934 cm^{-1}, the C═O stretching peak at 1650 cm^{-1}, the N—H bending peak at 1611 cm^{-1}, and the C—N stretching peaks at 1407 cm^{-1}) were clearly observed.[25] Also, the FTIR spectra of the p(AAm)–p(An) semi-IPN conductive cryogels showed characteristic peaks for both bare p(AAm) cryogels and electroconductive p(An). We observed a benzene–quinonic nitrogen peak at 1567 cm^{-1}, aromatic C—C peaks at 1496 cm^{-1}, an amine peak at 1357 cm^{-1}, C—N—C peaks at 1174 cm^{-1}, and C—H in-plane stretching at 1048 cm^{-1}; these were characteristic peaks for p(An) and were in accordance with the literature.[32]

The FTIR spectrum of the p(AMPS) and p(AMPS)–p(An) semi-IPN conductive cryogel composites are also given in Figure 4(b). As shown, the characteristic peaks of the p(AMPS) cryogels, such as the N—H stretching peaks from amide groups at 3435 and 3319 cm^{-1}, the aliphatic C—H peaks at 2987 and 2937 cm^{-1}, the C═O stretching peaks at 1648 cm^{-1}, O═S═O asymmetric stretching at 1366 cm^{-1}, O═S═O symmetric stretching at 1115 cm^{-1}, and S═O stretching vibrations at 1044 cm^{-1}, were clearly observed. Also, the characteristic peaks for p(An) are shown in the figure; these were similar to the p(An) peaks in the neutral network of the p(AAm) cryogel with

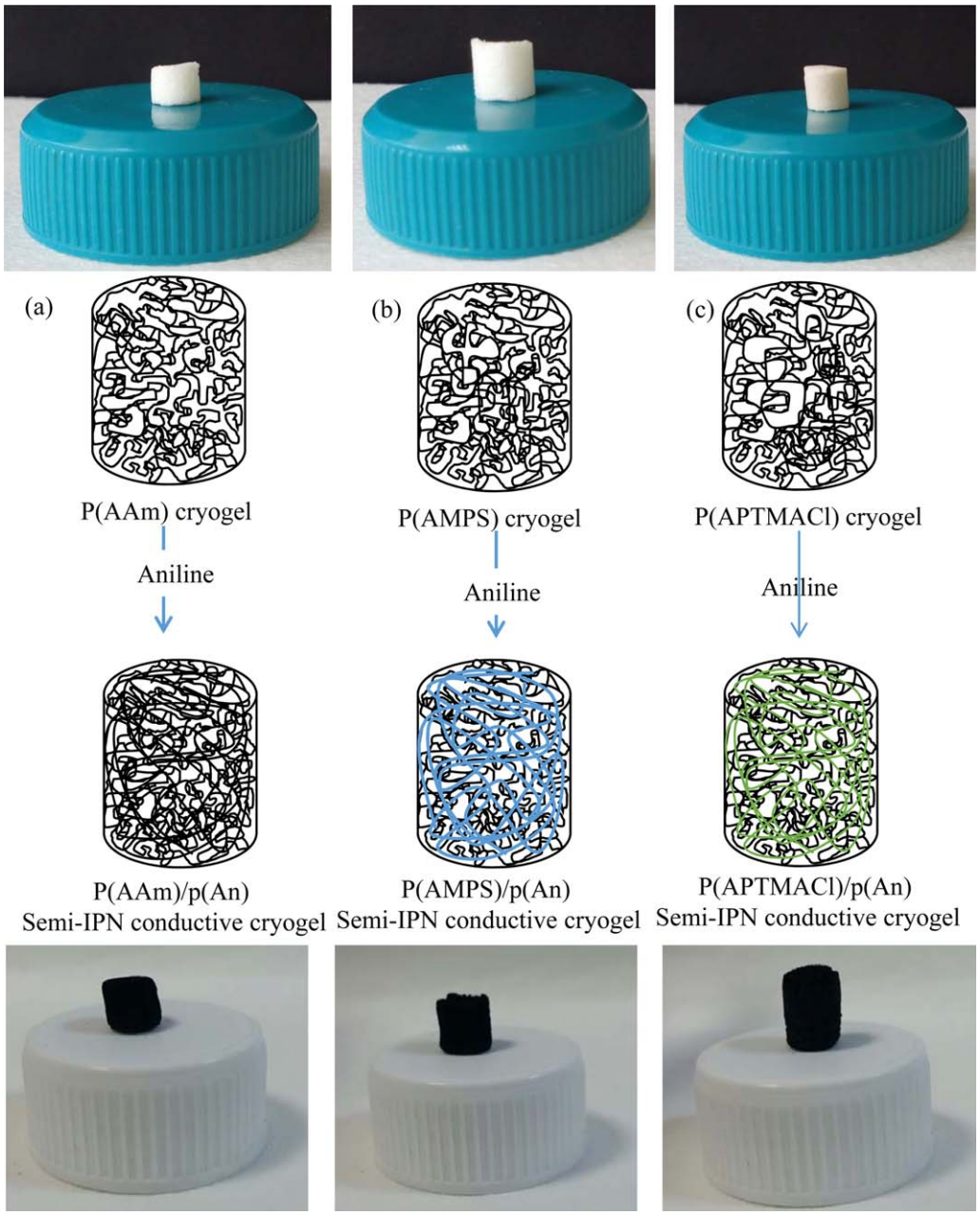

Figure 2. Digital camera images of the (a) p(Aam) and p(Aam)–p(An), (b) p(AMPS) and p(AMPS)–p(An), and (c) p(APTMACl) and p(APTMACl)–p(An) semi-IPN conductive cryogel composite systems. [Color figure can be viewed in the online issue, which is available at wileyonlinelibrary.com.]

some shifts because of the interaction of p(An) with the template of p(AMPS). The assigned benzene–quinonic nitrogen band at 1567 cm^{-1}, the aromatic C—C peaks at 1493 cm^{-1}, the aromatic amine band at 1351 cm^{-1}, the C—N—C peaks at 1214 cm^{-1}, and the C—H in-plane vibrations at 1025 cm^{-1} were also recognized.[35] In the FTIR spectra of the p(APTMACl) and p(APTMACl)–p(An) semi-IPN conductive cryogels shown in Figure 4(c), the functional groups were in accordance with the structure of conventional p(APTMACl) hydrogels that were reported in an earlier investigation.[27] For example, the N—H stretching modes of amide groups of APTMACl were observed at 3354 and 3247 cm^{-1}. Additionally, the C—H stretching of $—CH_3$ at 2942 cm^{-1}, the quaternized amine at 1640 cm^{-1}, N—H bending at 1540 cm^{-1}, C—H bending vibrations at 1480 cm^{-1}, and C—N—C stretching peaks at 1091 cm^{-1} were observed. After the *in situ* preparation of p(An) within the cationic cryogel network, again the characteristic peaks for p(An), such as those of benzene–quinonic nitrogen at 1569 cm^{-1}, the aromatic C—C at 1498 cm^{-1}, the aromatic amine at 1348 cm^{-1}, C—N—C at 1177 cm^{-1}, and C—H in-plane stretching at 1044 cm^{-1}, with some shifts were noticed.[35] Therefore, we concluded that the p(An) conducting polymer was readily prepared within the superporous neutral, anionic, and cationic networks of the AAm-based cryogels.

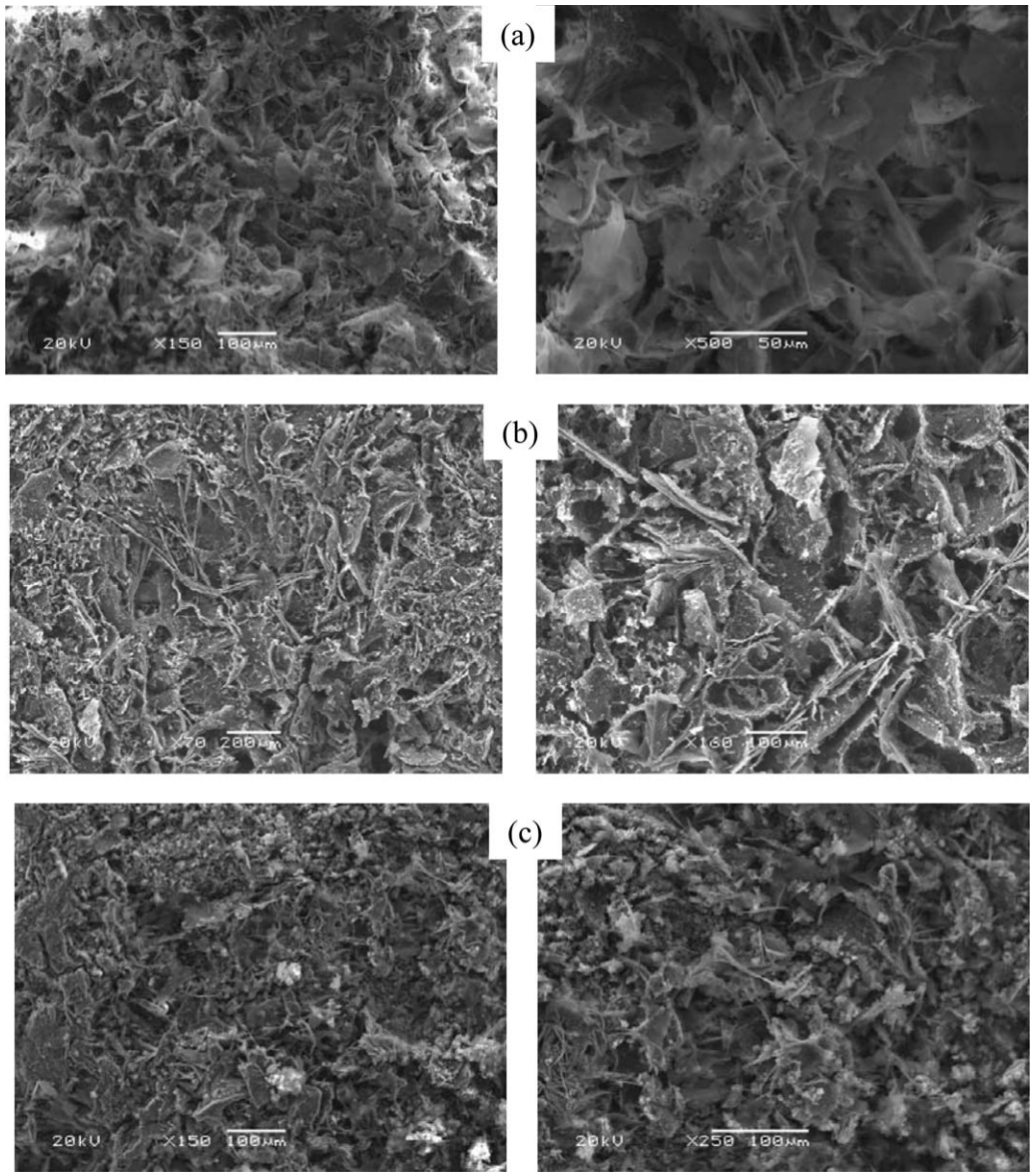

Figure 3. SEM images of the (a) p(Aam)–p(An), (b)p(AMPS)–p(An), and (c) p(APTMACl)–p(An) semi-IPN conductive cryogel composite systems.

Electroconductive Properties of the p(AAm)–p(An), p(APTMACl)–p(An), and p(AMPS)–p(An) Semi-IPN Conductive Cryogel Composites

Each component of the cryogel–CP composites has attracted tremendous attention in research and technological applications because of their superporosity, elasticity, flexibility, high mechanical strength, fast responsiveness,[24–27] and electronically active and conducting nature of p(An).[5] The lone electron pairs on nitrogen participate in conjugation, and the doping is associated with a chain protonation mechanism in p(An) that leads to electronic conductions. Because of its low cost, chemical stability, and electronic properties, p(An) is the among the most widely investigated electrical CPs for various application, such as those in electronics, opto-electronics devices, sensors, and medicine.[15–17] Therefore, the synthesized electroconductive p(An) within various functional groups containing cryogels that are used as templates, such as nonionic p(AAm), anionic p(AMPS), and cationic p(APTMACl) cryogels, can offer synergistic properties for advanced sensor design with great potential. The schematic presentation of setup for the electrical conductivity measurements from the current–voltage curves of the bare p(AAm), p(AMPS), and p(APTMACl) cryogels and their corresponding p(AAm)–p(An), p(AMPS)–p(An), and p(APTMACl)–p(An) semi-IPN conductive cryogel composites at room temperature are given in Figure 5(a). The cylindrical shapes of the cryogel samples, p(AAm) (diameter = 5 mm and length = 5.5 mm), p(AMPS) (diameter = 5 mm and length = 3.5 mm), and p(APTMACl) (diameter = 5 mm and length = 4.5 mm), were used in conductivity measurements through the attachment of carbon tape ($0.5 \times 0.5\ cm^2$) at the top and bottom sides of the cylindrical cryogels. Before the current–voltage curves were obtained, the cylindrical cryogels were dried at 70 °C in a vacuum oven for 12 h. The bulk resistance (R) values of the p(AAm), p(AMPS), and p(APTMACl) cryogels and the p(AAm)–p(An), p(AMPS)–p(An), and p(APTMACl)–p(An) semi-IPN conductive cryogels were calculated from the applied

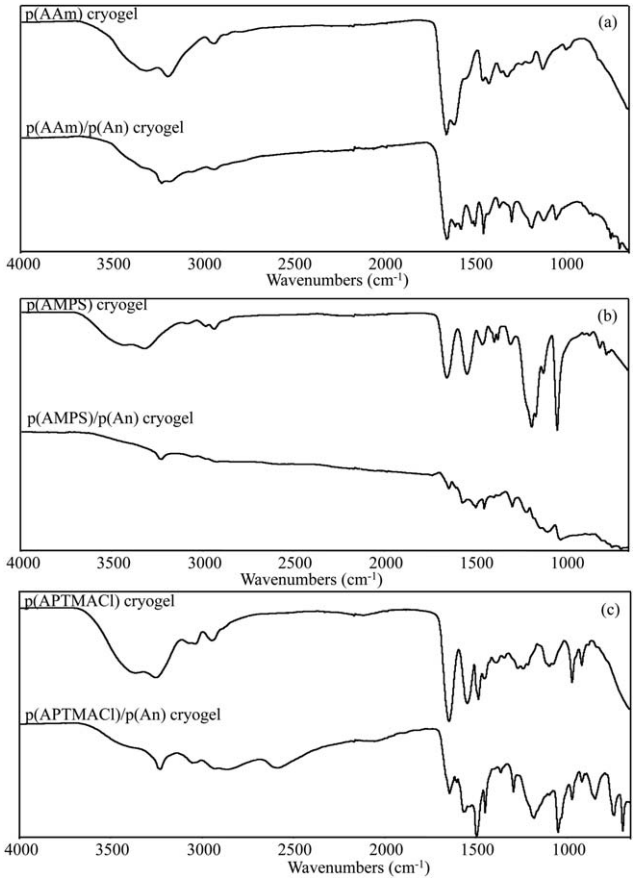

Figure 4. FTIR spectra of the (a) bare p(Aam) and p(Aam)–p(An), (b) bare p(AMPS) and p(AMPS)–p(An), and (c) p(APTMACl) and p(APTMACl)–p(An) semi-IPN conductive cryogel systems.

voltage and recorded current with Ohm's law via multiple separate measurements that were performed on each sample. The conductivities were calculated from the slope of the Ohmic regions of the current–voltage curve for each bare cryogel; the p(AAm), p(AMPS), and p(APTMACl) cryogels; and the p(AAm)–p(An), and p(AMPS)–p(An), p(APTMACl)–p(An) semi-IPN conductive cryogel composites via eq. (1):

$$\text{Conductivity} = (1/R) \times (L/A) \quad (1)$$

where L is the length and A is the cross-sectional area of the sample. The current–voltage curves of the bare p(AAm), p(AMPS), and p(APTMACl) cryogels were measured and are illustrated in Figure 5(b). The resistance values of the p(AAm), p(AMPS), and p(APTMACl) cryogels were calculated from the current–voltage curves, and the highest resistance value was observed for the nonionic p(AAm) cryogels with 1×10^{10} Ω. The resistance values for the anionic p(AMPS) and cationic p(APTMACl) cryogels were measured as 2×10^{6} and 1.4×10^{5} Ω, respectively. Because of the anionic and cationic nature of these cryogels, it was reasonable to assume that the ionic conductivity contributed to the lower resistance in comparison to that of the neutral p(AAm) cryogels. The conductivities of the bare p(AAm), p(AMPS), and p(APTMACl) cryogels were calculated with eq. (1), and the corresponding graph is given in Figure 5(c). The ionic anionic p(AMPS) and cationic p(APTMACl) cryogels had $7 \times 10^{-6} \pm 3 \times 10^{-7}$ and $1.3 \times 10^{-4} \pm 7 \times 10^{-6}$ S/cm conductivity values, whereas the conductivity values of the p(AAm) cryogels ($2.2 \times 10^{-9} \pm 1 \times 10^{-10}$ S/cm) were approximately 3×10^{3} and 6×10^{5} times lower than the conductivities of the p(AMPS) and p(APTMACl) cryogels, respectively. The cationic p(APTMACl) cryogels showed a higher conductivity than the anionic p(AMPS) cryogels; this could be attributed to the existence of mobile Cl^{-} ions.

Furthermore, the current–voltage curves of the p(AAm)–p(An), p(AMPS)–p(An), and p(APTMACl)–p(An) semi-IPN conductive cryogels were measured, and the corresponding current–voltage curves are given in Figure 6(a). The resistance values calculated from the current–voltage curves for the p(AAm)–p(An), p(AMPS)–p(An), and p(APTMACl)–p(An) semi-IPN conductive cryogel composites were lower than those of the bare p(AAm), p(AMPS), and p(APTMACl) cryogels, with values of 2×10^{3}, 2×10^{3}, and 5×10^{3} Ω, respectively. The decrease in the resistance values of the p(AAm), p(AMPS), and p(APTMACl) cryogels upon the inclusion of p(An) within the corresponding cryogels provided higher electrical conductivities for the p(AAm)–p(An), p(AMPS)–p(An), and p(APTMACl)–p(An) semi-IPN conductive cryogel composites. The comparison of

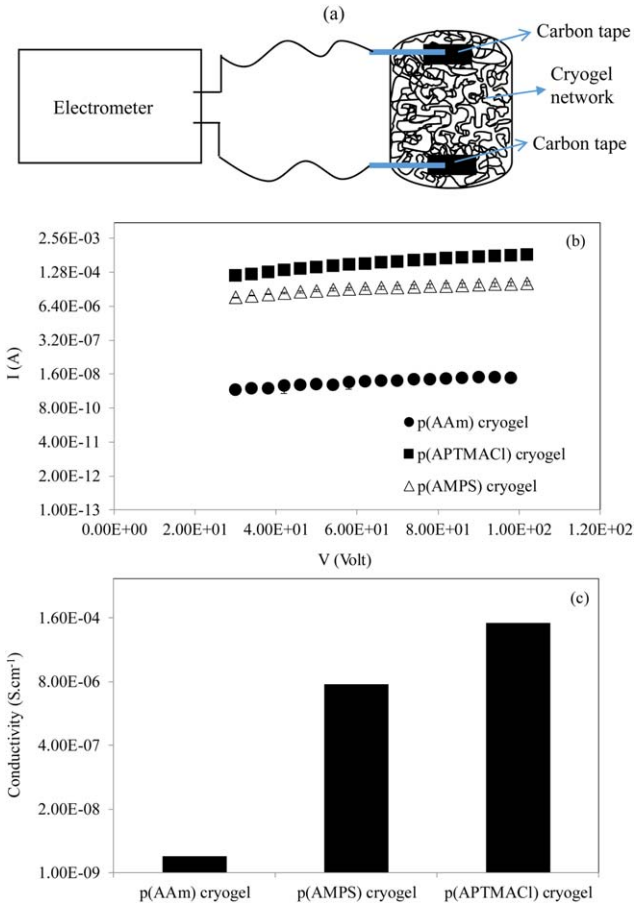

Figure 5. (a) Scheme of the conductivity measurement setup; (b) current (I)–voltage (V) curves for the bare p(AAm), p(AMPS), and p(APTMACl) cryogels; and (c) corresponding conductivity values. [Color figure can be viewed in the online issue, which is available at wileyonlinelibrary.com.]

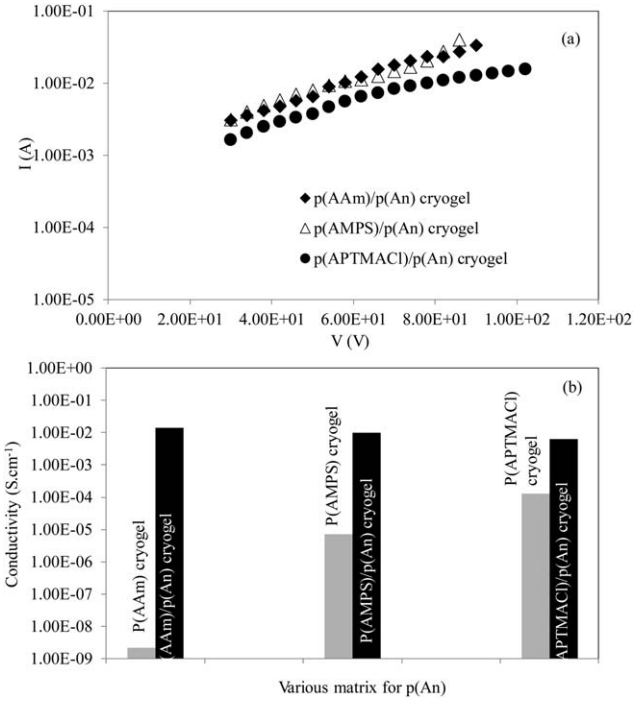

Figure 6. (a) Ohmic region of the current (*I*)–voltage (*V*) curves of p(Aam)–p(An), p(AMPS)–p(An), and p(APTMACl)–p(An) semi-IPN conductive cryogel composite systems and (b) comparison of the conductivity values of the p(AAm)–p(An), p(AMPS)–p(An), and p(APTMACl)–p(An) semi-IPN conductive cryogel systems with their bare forms [p(AAm), p(AMPS), and p(APTMACl) cryogels, respectively].

the conductivities of the bare p(AAm), p(AMPS), and p(APTMACl) cryogels with their corresponding p(AAm)–p(An), p(AMPS)–p(An), and p(APTMACl)–p(An) semi-IPN cryogels is illustrated in Figure 6(b). As we clearly observed, the conductivities of the bare p(AAm), p(AMPS), and p(APTMACl) cryogels increased approximately 6.4×10^6 fold for the p(AAm)cryogels, 1.3×10^3 fold for the p(AMPS) cryogels, and 5×10^1 fold for the p(APTMACl) cryogels with the synthesis of p(An) CP within cryogels with $1.4 \times 10^{-2} \pm 4 \times 10^{-4}$, $1 \times 10^{-2} \pm 2 \times 10^{-4}$. and $6.4 \times 10^{-3} \pm 2.4 \times 10^{-5}$ S/cm for the p(AAm)–p(An), p(AMPS)–p(An), and p(APTMACl)–p(An) semi-IPN conductive cryogel composites, respectively. Here, the positive effect of p(An) on the conductivity of the p(AAm)-p(An) cryogels was observed. It was apparent that the electrical conductivity of the cryogels primarily depended on the existence of p(An) chains. The conductivity was mainly dependent on the concentration and mobility of the charge carriers: polarons and bipolarons. These carriers were mobile in an electric field, and they were responsible for electrical conduction along the polymer chain. The most accepted mechanism in electrical conductivity is the charge transportation along the p(An) chains and the hopping of carriers from chain to chain. Therefore, the polymerization of An in the superconnected and interconnected cryogel network produced free radicals and polarons, and the presence of polarons on the chain introduced localized electronic levels in the band gap. This led to an increase in the electrical conductivity of the cryogel–CP composite materials. The very high conductivity values are not important especially for materials that are used in sensor applications, as the higher the conductivity, the lower the sensitivity and hence the lower the detection limit is most probable outcome. Therefore, even changes in the conductivities of the prepared cryogels were measured and used in the design of different sensor applications; the prepared cryogels offered a higher sensitivity than conventional hydrogels as the cryogel network responded faster to external stimuli than conventional hydrogels. Furthermore, the combination of cryogels with CPs, such as p(An), in the form of semi-IPN conductive composite cryogel network, could make these versatile materials promising advanced sensor devices because of the combinatory effect of both components.

CONCLUSIONS

Here, we demonstrated that the p(An) CPs within superconnected and interconnected porous cryogels with the neutral p(AAm), anionic p(AMPS), and cationic p(APTMACl) cryogels were successfully synthesized via an oxidative polymerization method. The SEM and FTIR measurements clearly confirmed the existence of p(An) within the pores of templates, and this confirmed the preparation of the p(AAm)–p(An), p(AMPS)–p(An), and p(APTMACl)–p(An) semi-IPN conductive cryogel composites. Moreover, the conductivity values of 7×10^{-6} and 1.3×10^{-4} S/cm for the anionic p(AMPS) and cationic p(APTMACl) cryogels were calculated; these values were much higher than the conductivity value of the nonionic p(AAm) cryogels with $2.2 \times 10^{-9} \pm 1 \times 10^{-10}$ S/cm values. The anionic p(AMPS) and cationic p(APTMACl) cryogels provided a higher ionic conductivity then the nonionic p(AAm) cryogels. Furthermore, upon the preparation of p(An) in the cryogel network, the electrical conductivities increased significantly. Interestingly, p(AAm)–p(An) semi-IPN conductive cryogel composites with a $1.4 \times 10^{-2} \pm 4 \times 10^{-4}$ S/cm conductivity; this was 6.4×10^6 fold higher than the values of the bare p(AAm) cryogels and showed the highest conductivity. On the other hand, the conductivities of the p(AMPS)–p(An) and p(APTMACl)–p(An) semi-IPN conductive cryogels also increased when compared to the bare forms of the p(AMPS) and p(APTMACl) cryogels with $1 \times 10^{-2} \pm 2 \times 10^{-4}$ and $6.4 \times 10^{-3} \pm 2.4 \times 10^{-5}$ S/cm; this corresponded to almost 1.3×10^3 and 5×10^1 fold increases in their conductivity values, respectively. It was obvious that the presence of CP in the network increased the conductivities of the bare p(AAm), p(AMPS), and p(APTMACl) cryogels. The highest increase in the p(AAm)–p(An) semi-IPN conductive cryogel composites could have been due to the relatively fewer interactions of p(An) with neural network in comparison to its high interaction possibility with the charged anionic and cationic networks of cryogels. Therefore, the synthesis of the p(An) cryogel in the pores of various cryogel networks with different functional groups and charges can open up new opportunities for the applications of these cryogel–CP composites in the design of novel biomedical devices for sensors, electrically controlled drug-delivery systems, actuator systems for implants, and so on.

ACKNOWLEDGMENTS

This work was supported by the Scientific and Technological Research Council of Turkey (contract grant number 214M130).

REFERENCES

1. Small, C. J.; Too, C. O.; Wallace, G. G. *Polym. Gels Networks* **1997**, *5*, 251.
2. Guiseppi-Ellie, A.; Wilson, A. M.; Sujdak, A. R.; Brown, K. E. *Polym. Prepr.* **1997**, *98*, 608.
3. Heeger, A. *Synth. Met.* **2002**, *125*, 23.
4. Shirakawa, H. *Angew. Chem. Int. Ed.* **2001**, *40*, 2575.
5. Dispenza, C.; Sabatino, M. A.; Niconov, A.; Chmielewska, D.; Spadaro, G. *Radiat. Phys. Chem.* **2012**, *81*, 1456.
6. George, P. M.; Lyckman, A. W.; LaVan, D. A.; Hegde, A.; Leung, Y.; Avasare, R.; Testa, C.; Alexander, P. M.; Langer, R.; Sur, M. *Biomaterials* **2005**, *26*, 3511.
7. Giraldo, C. T.; Kelly, A.; Biggs, M. J. P. *Drug Discovery Today* **2014**, *19*, 88.
8. Hardy, J. G.; Lee, J. Y.; Schmidt, C. E. *Curr. Opin. Biotechnol.* **2014**, *24*, 847.
9. Justin, G.; Finley, S.; Abdurrahman, A. R.; Guiseppi-Elie, A. *Biomed. Microdevices* **2009**, *11*, 103.
10. Krukiewicz, K.; Zawisza, P.; Herman, A. P.; Turczyn, R.; Boncel, S.; Zak, J. K. *Bioelectrochemistry* **2016**, *108*, 13.
11. Tsai, N. C.; Sue, C. Y. *Sens. Actuators A* **2008**, *141*, 670.
12. Puguan, J. M. C.; Chung, W. J.; Kim, H. *Electrochim. Acta* **2016**, *196*, 236.
13. Unsworth, N. K.; Hancox, I.; Dearden, C. A.; Sullivan, P.; Walker, M.; Lilley, R. S.; Sharp, J.; Jones, T. S. *Org. Electron.* **2014**, *15*, 1624.
14. Mohsennia, M.; Bigdoli, M. M.; Boroumand, F. A.; Nia, A. M. *Mater. Sci. Eng. B* **2015**, *197*, 25.
15. Gospodinova, N.; Terlemezyan, L. *Prog. Polym. Sci.* **1998**, *23*, 1443.
16. Bhadra, S.; Khastgir, D.; Singha, N. K.; Lee, J. H. *Prog. Polym. Sci.* **2009**, *34*, 783.
17. Bagherzadeh, M. R.; Ghasemi, M.; Mahdavi, F.; Shariatpanahi, H. *Prog. Org. Coat.* **2011**, *72*, 348.
18. Osada, Y.; Okuzaki, H.; Hori, H. *Nature* **1992**, *355*, 242.
19. Altava, B.; Compan, V.; Andrio, A.; del Castillo, L. F.; Molla, S.; Burguete, M. I.; Garcia-Verdugo, E.; Luis, S. V. *Polymer* **2015**, *7*, 69.
20. Matsumoto, K.; Endo, T. *React. Funct. Polym.* **2013**, *73*, 278.
21. Siddhanta, S. K.; Gangopadhyay, R. *Polymer* **2005**, *46*, 2993.
22. Dispenza, C.; Lo Presti, C.; Belfiore, C.; Spadaro, G.; Piazza, S. *Polymer* **2006**, *47*, 961.
23. Zhao, Y.; Liu, B. R.; Pan, L. J.; Yu, G. H. *Energy Environ. Sci.* **2013**, *6*, 2856.
24. Lozinsky, V. I.; Okay, O. *Adv. Polym. Sci.* **2014**, *263*, 49.
25. Seven, F.; Sahiner, N. *J. Power Sources* **2014**, *272*, 128.
26. Sahiner, N.; Seven, F. *RSC Adv.* **2014**, *4*, 23886.
27. Sahiner, N.; Demirci, S.; Sahiner, M.; Yilmaz, S.; Al-Lohedan, H. *J. Environ. Manage.* **2015**, *152*, 66.
28. Bloch, K.; Vanichkin, A.; Damshkaln, L. G.; Lozinsky, V. I.; Vardi, P. *Acta Biomater.* **2010**, *6*, 1200.
29. Ertürk, G.; Mattiasson, B. *J. Chromatogr. A* **2014**, *1357*, 24.
30. Arvidsson, P.; Plieva, F. M.; Lozinsky, V. I.; Galaev, I. Y.; Mattiasson, B. *J. Chromatogr. A* **2003**, *986*, 275.
31. Fatoni, A.; Numnuam, A.; Kanatharana, P.; Limbut, W.; Thammakhet, C.; Thavarungkul, P. *Sens. Actuators B* **2013**, *185*, 725.
32. Karacan, P.; Okay, O. *React. Funct. Polym.* **2013**, *73*, 442.
33. Sahiner, N.; Yildiz, S.; Al-Lohedan, H. *Appl. Catal. B* **2015**, *166*, 145.
34. Sahiner, N.; Seven, F. *Fuel Process. Technol.* **2015**, *132*, 1.
35. Vera, R. A.; Romero, B. H.; Ahumada, E. *J. Chil. Chem. Soc.* **2003**, *48*, 1.